Energy Reports 6 (2020) 1043–1056

Contents lists available at ScienceDirect

Energy Reports

journal homepage: www.elsevier.com/locate/egyr

Research paper

Multi-site measurement for energy application of small distributed wind farm in complex mountainous areas

Mingjin Zhang [a], Jingyu Zhang [a,*], Yongle Li [a], Jiaxin Yu [a], Jingxi Qin [b], Kai Wei [a], Lili Song [c]

[a] Department of Bridge Engineering, Southwest Jiaotong University, Chengdu, Sichuan 610031, China
[b] Department of Civil and Environmental Engineering, University of California, Los Angeles, CA 90024, USA
[c] Public Meteorological Service Center, China Meteorological Administration, Beijing 100081, China

ARTICLE INFO

Article history:
Received 16 October 2019
Received in revised form 13 February 2020
Accepted 8 April 2020
Available online xxxx

Keywords:
Wind energy
Complex mountainous region
Mountainous wind characteristics
Weibull distribution
Multi-site measurement
Extreme value analysis

ABSTRACT

As a clean and highly valuable renewable energy, wind energy has gradually become an important branch of energy technology. By means of measurement methods, the wind characteristics, energy applications for distributed wind energy source (DWES) in six sites in Henduan Mountains and economic evaluation are investigated. According to the results, the wind characteristics including wind speed and wind direction in mountainous regions are affected significant by topography. Wind speed is season-dependent, while the mean wind direction is not. The maximum wind speed occurs in spring, the minimum wind speed occurs in summer. As for extreme value distribution, the wind data in mountainous areas are more in line with Frechet distribution type. By using Weibull distribution function, Weibull parameters are calculated and energy potential are estimated with five methods. Estimation methods suitable for coastal areas can also be used for energy assessment in mountain environments. The maximum wind power density is over 200 W/m^2, occurred in Zanli site, while the minimum value is less than 10 W/m^2 in Yimen-A. Similar to mean wind characteristics, wind power density shows strong seasonality, with the maximum value in spring and the lowest value in summer. In addition, power generation facilities should be built in valleys or on the top of the mountain, and should not be built in the flat land surrounded by mountains. And the total cost of 1kWh wind-generated electricity is 0.305 CNY/kWh and 0.406 CNY/kWh with different type of wind turbine.

1. Introduction

Renewable energy, which includes hydropower, solar, wind, wave, geothermal, etc., is a kind of sustainable energy supply that can meet the current energy demand without harming the environment. Among these energy sources, widely distributed and with many policies support and financial incentives from governments, wind energy has received a lot of attention and undergone rapid development including wind energy estimate method and wind speed prediction (Fyrippis et al., 2010; Jiang et al., 2019; Peng et al., 2017). Fig. 1 shows the cumulative installed wind power capacity and new installed wind power capacity per year from 2006 to 2018 (Global Wind Energy Council, 2019). By the end of 2018, the cumulative installed wind power capacity in the world has reached 591.5 GW. Over the past 13 years, the new installed capacity has experienced two upsurges and has stabilized at 52GW per year in the last three years. Top 10 countries in newly installed wind power capacity in 2018 is shown in Fig. 2. As shown, developing countries contribute more than half of the new installed capacity.

After decades of development, there have been many studies on the wind characteristics and wind energy assessment of large wind farms built in coastal areas and offshore areas. Aiming at offshore areas, Shu et al. explored the offshore wind characteristics and estimated the wind power potential in Hongkong by calculating Weibull parameters with different estimation methods (Shu et al., 2015a,b). Soon after, Shu et al. investigated the wind energy potential at different height in different locations in Hong Kong, and pointed that the Weibull shape parameter is height-independent, whereas the Weibull scale parameters demonstrate a power-law type in height in offshore region (Shu et al., 2016). In Turkey, two wind masts with the height of 30 m were erected in Kutahya, an inland area, and Izmir, a coastal area, respectively. According to the data collected, the mean wind speed in Izmir is 8.14 m/s while the mean wind speed in Kutahya is 4.62m/s, which indicates that the wind characteristics is affected by the

* Corresponding author.
E-mail addresses: Zhang-Minjin@swjtu.edu.cn (M. Zhang), zhangjycd@live.com (J. Zhang), lele@swjtu.edu.cn (Y. Li), jxyu0521@gmail.com (J. Yu), qinjx@g.ucla.edu (J. Qin), swjtu_kw@163.com (K. Wei), songll@cma.gov.cn (L. Song).

https://doi.org/10.1016/j.egyr.2020.04.019

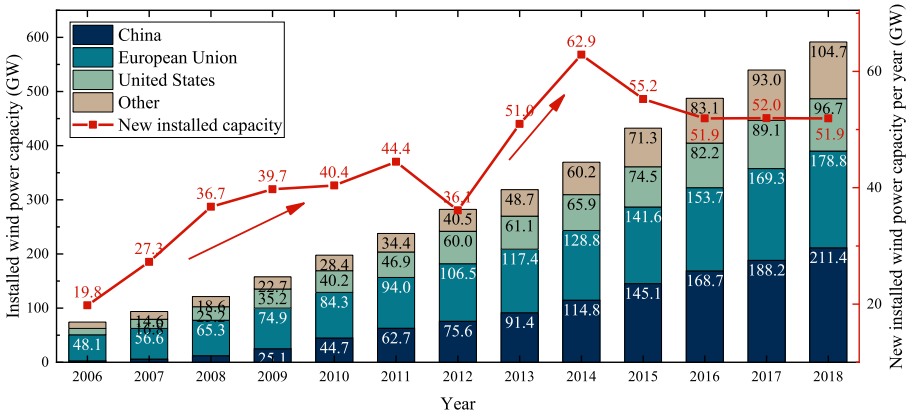

Fig. 1. Installed wind power capacity around the world from 2006 to 2018.

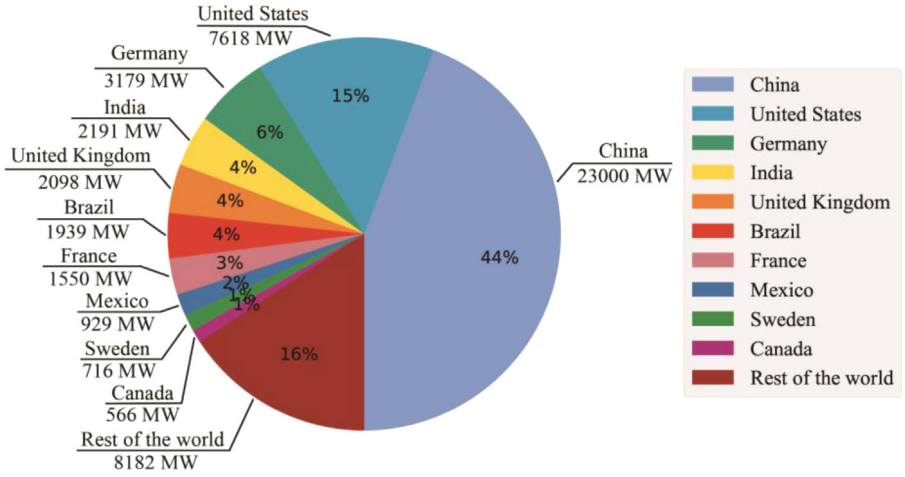

Fig. 2. Top 10 countries in newly installed wind power capacity in 2018 (Unit: MW).

topography (Kose et al., 2004; Köse, 2004). Besides, because the relationship between wind energy density and wind speed is cubic, assuming that under the same other conditions, the wind energy density in Izmir is about five times that in Kutahya, it can be seen that wind speed is very important for the location of wind power stations. In recent years, with the progress of wind power technology, miniaturized horizontal axis wind turbines (HAWTs) and more advanced vertical axis wind turbines (VAWTs) have been developed, researches on distributed wind energy source (DWES) are becoming a hot topic. DWES is a decentralized energy supply mode built at the user end, which can operate independently as well as in the grid. Although the power generation of DWES is small, it can maximize the use of resources and environmental benefits (Bayod-Rújula, 2009; Kaundinya et al., 2009). Lu and Ip (2009) investigated the feasibility of wind power generation installed on high-rise buildings in Hongkong by CFD method, and this assumption had also been proved theoretically. Aiming at capital circle of Malaysia, a DWES system built on the roof of high-rise buildings was proposed and discussed, the results showed that the DWES system can cover a signification portion of a building's energy demand and helps to make the building partially independent from the urban electricity grid (Chong et al., 2013, 2011). Based on the assessment of wind energy potential in different parts of Singapore, the feasibility of wind energy in the city is further confirmed (Karthikeya et al., 2016). In addition, a large number of scholars have discussed the application of DWES system in the modern city (Chong et al., 2011; Kumar et al., 2018; Pagnini et al., 2015).

Through the review of the above literatures, it can be found that there are many researches on large-scale wind farms in offshore areas or onshore area with open land and DWES systems in large modern cities. But as we know, the complex mountainous regions, such as Rocky Mountains in U.S., Henduan Mountains in China, Zagros Mountains in Iran, etc., are widely distributed in the world and a large number of people are gathering here. And it is uneconomical to build power stations or transmission lines specifically for these underdeveloped areas in such extreme conditions (Ti et al., 2020, 2019; Zhang et al., 2019a). The expensive power system does not match the level of local economic development. Hence, DWES system can provide new ideas and solutions to solve the energy demand of remote mountainous areas. For some places with plenty of sunshine, DWES systems and solar energy can be combined into a hybrid power system to obtain more electricity (Allan et al., 2015; Khare et al., 2016). Therefore, the assessment of wind energy potential in remote mountainous areas can provide references for DWES. From the perspective of solving the local energy supply problem in remote mountain areas, four remote villages with six wind measurement sites in Henduan Mountains are selected as the research objects to investigate the wind energy application of DWES. The results are expected to provide useful information for the development of distributed energy resources and the application of DWES in valleys. This paper is organized as follow: Section 2 gives detailed information about the four places with six wind sites and the methods used in this paper to analyze the wind data. Section 3 presents the analysis and comparison of the mean wind characteristics, return level, Weibull characteristics, assessment of wind

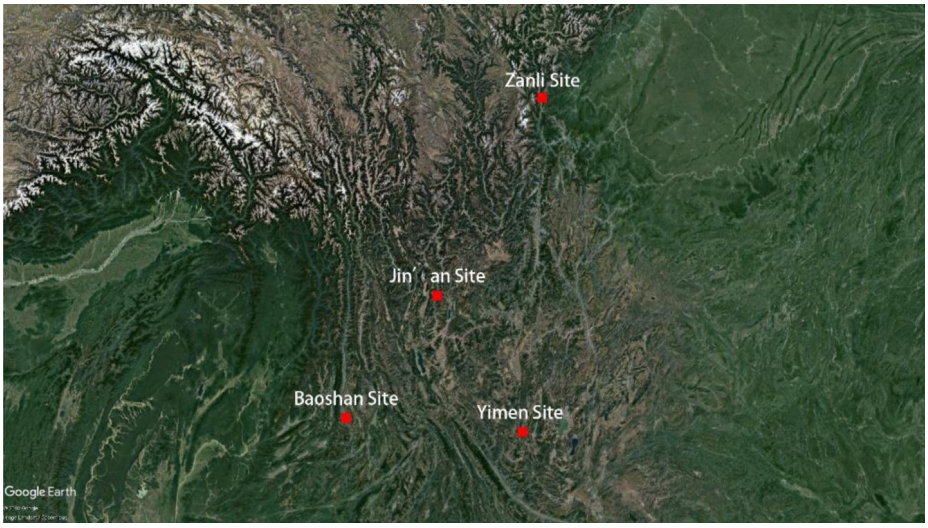

Fig. 3. Topographic maps for four measuring stations (Captured from Google Earth).

potential at different sites and economic evaluation. Section 4 summarizes the conclusions.

2. Methodology

2.1. Measurement sites

Hengduan Mountains, located in the southwestern China, is the border mountain system of the Qinghai-Tibet Plateau and Yunnan-Guizhou Plateau, covering an area of more than 600,000 square kilometers. It is the longest, widest, and most typical north–south mountain system in China (Xing and Ree, 2017). Elevations of most land in this region ranges from 1300 to 6000 meters above sea level, and the elevation difference between mountains and adjacent valleys is generally over 1000 to 2000 m. In this paper, a total of 4 stations including 6 weather monitor stations were built to measure the wind data (see Figs. 3 and 4). The four stations are Zanli site, Jin'an site, Baoshan site and Yimen site in turn. Zanli site and Jin'an site are U-shaped deep-cut canyons situated on the eastern boundaries and central of the Hengduan Mountains, respectively. Baoshan site is located at the southwest boundary of Hengduan Mountains, where the terrain is relatively flat. In order to investigate the influence of topography on wind characteristics and energy potential assessment, three sites, Yimen-A, Yimen-B and Yimen-C, were set up in three adjacent areas of Yimen with different topography. Yimen-A, Yimen-B, and Yimen-C are located on the flat land surrounded by mountains, at the top of a low hillside near the flat land, and in the valley nearby.

2.2. Wind data measurement mast

Each automatic weather station used in the observation is a 10 m high mast (see Fig. 5). The mast is composed of steel circular tubes, strengthened by serval guyed wires to enhance the stability. In addition, the mast is equipped with lightning protection equipment to maximize the service life of the instruments. In wind field measurements, cup-anemometer is usually selected as the standard acquisition instrument for its simple installation and high accuracy (Khan and Tariq, 2018; Kristensen, 1999, 1998). Therefore, a 3-cup anemometer and a direction sensor are equipped at the top of the mast. At the bottom of the mast, a thermometer and a rainfall sensor are installed to record the temperature data and rainfall data. All data will be recorded in real time by the data logger and transmitted to the remote data center via cellular data. Finally, a large capacity battery which endurance is 72 h and charged by the solar panels is used to power the entire automatic weather station. And the collection duration of wind data is from December 2012 to December 2018. The sampling frequency of each sensor is 1 Hz, and the recorded data is 10 min mean wind speed. Due to the influence of climate, instrument failure and other factors, missing data and distortion data are inevitable. Therefore, the 3σ principle is used to judge the distortion data, and the interpolation method to complete the missing and distortion data. After checking all the data used in this paper, the data missing rate of all instruments is less than 5%.

2.3. Extreme value analysis

Extreme value analysis, also known as extreme value theory, is a statistical method used to deal with the extreme deviation of the median of probability distribution (Castillo, 1988). For a given independent and identically distributed random variables, extreme value analysis can evaluate the probability of more extreme events from sample sequences than previously observed (Kruyt et al., 2017). Supposed the length of the samples is large enough, the probability can be obtained by the GEV distribution, whose probability density function (PDF) and cumulative distribution function (CDF) is given by Eqs. (1) and (2) respectively (Jenkinson, 1955).

$$g(v;\mu,\alpha,\xi) = \frac{1}{\alpha}\left(1+\xi\left(\frac{v-\mu}{\alpha}\right)\right)^{-\frac{\xi+1}{\xi}} \exp\left(-\left(1+\xi\left(\frac{v-\mu}{\alpha}\right)\right)^{-\frac{1}{\xi}}\right) \tag{1}$$

$$G(v;\mu,\alpha,\xi) = \exp\left(-\left(1+\xi\left(\frac{v-\mu}{\alpha}\right)\right)^{-\frac{1}{\xi}}\right) \tag{2}$$

where μ, σ and ξ are the location, scale and shape parameter, respectively. Depending on the value of ξ, GEV can be divided into three types (de Oliveira et al., 2011): Type I extreme value distribution (Gumbel distribution, $\xi = 0$), Type II extreme value distribution (Frechet distribution, $\xi < 0$) and Type III extreme value distribution (Reversed Weibull distribution, $\xi > 0$).

The return level, a value is defined as that is expected to be equaled or exceeded on average once every interval of period

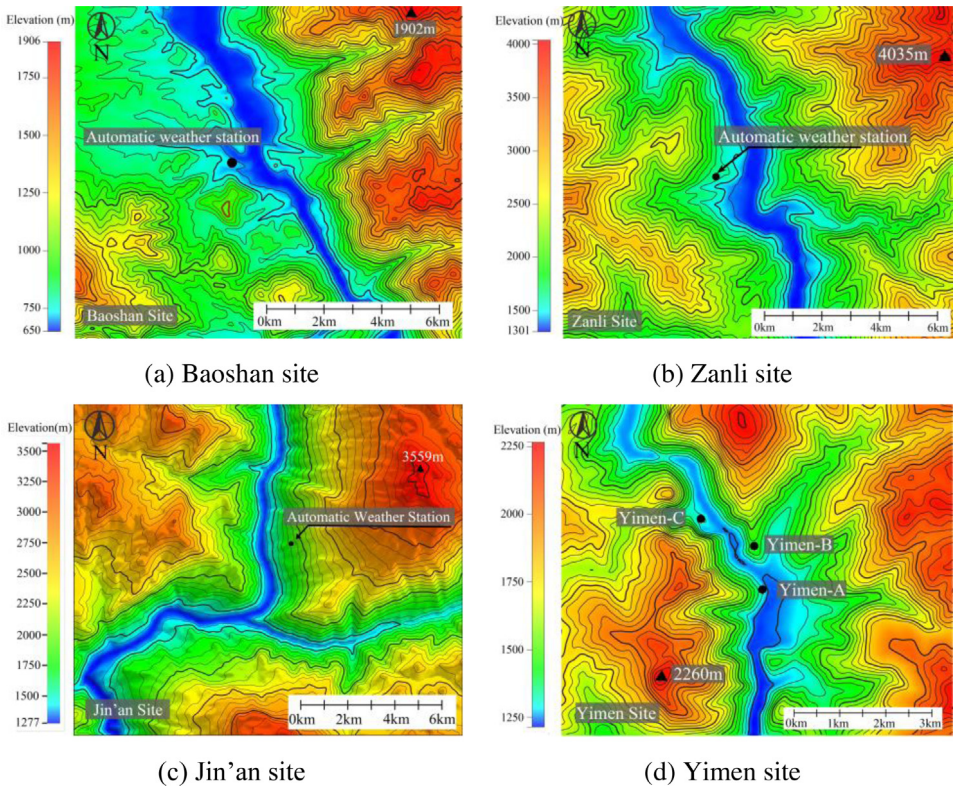

Fig. 4. Elevation indication of each station and relative position of each measured site.

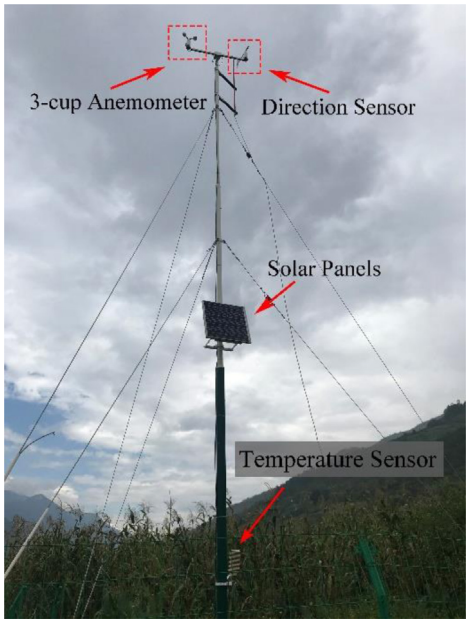

Fig. 5. The automatic weather station at Jin'an site (Photo by authors).

(P_0), can be calculated to estimate the occurrence probability of extreme quantiles. Here, the P_0 is called return period, the return level can be obtained as the following equation (Perrin et al., 2006):

$$G(x) = 1 - \frac{1}{P_0} \tag{3}$$

2.4. Weibull distribution of wind data

Wind is a random variable in time and space, so it is very difficult to evaluate it and more reasonable to use statistical analysis method to evaluate the potential of wind energy, rather than instantaneous wind data (Shu et al., 2016). Therefore, the two-parameter Weibull distribution, which is widely used in wind energy potential assessment, is used to analyze and evaluate the wind data (Carneiro et al., 2016; Cost Rocha et al., 2012; Lee et al., 2015). The corresponding mathematical expressions of PDF and CDF are presented as Eqs. (4) and (5) respectively.

$$w(v; k, c) = \frac{k}{c}\left(\frac{v}{c}\right)^{k-1} \exp\left(-\left(\frac{v}{c}\right)^{k}\right) \tag{4}$$

$$W(v; k, c) = 1 - \exp\left(-\left(\frac{v}{c}\right)^{k}\right) \tag{5}$$

Where, $w(v)$ and $W(v)$ represent the PDF and the CDF, respectively. k is the dimensionless Weibull shape parameter and c is the Weibull scale parameter. Since the Weibull function is used in the offshore field, in order to examine the applicability of different estimate methods in complex mountain areas, we introduce five numerical methods to estimate the two Weibull parameters: empirical method, moment method, maximum likelihood method, energy pattern factor method and alternative maximum likelihood method (Chang, 2011; Chaurasiya et al., 2018; Cost Rocha et al., 2012).

Maximum likelihood method (Weibull-MLM) is the most widely used method, it is usually necessary to determine the parameters of Weibull distribution by numerical iteration (Fisher, 1915). Based on this method, Weibull shape and scale parameters are calculated by:

$$k = \left[\frac{\sum_{i=1}^{n} v_i^k \ln(v_i)}{\sum_{i=1}^{n} v_i^k} - \frac{\sum_{i=1}^{n} \ln(v_i)}{n}\right]^{-1} \tag{6}$$

$$c = \left(\frac{1}{n}\sum_{i=1}^{n} v_i^k\right)^{1/k} \tag{7}$$

Moment method (Weibull-MM) is an alternative to the maximum likelihood method (Justus and Mikhail, 1976), and the Weibull parameters can be obtained by the following expression:

$$v_m = c\Gamma(1+1/k) \tag{8}$$

$$\sigma = c\left[\Gamma(1+2/k) - \Gamma^2(1+1/k)\right]^{1/2} \tag{9}$$

Where σ is the standard deviation of the wind speed, v_m is the mean wind speed, and $\Gamma()$ is the Gamma function expressed by:

$$\Gamma(x) = \int_0^{\infty} t^{x-1}\exp(-t)dt \tag{10}$$

Empirical method (Weibull-EM) is a special case of the moment method, and the parameter k and c can be determined by the following equations:

$$k = \left(\frac{\sigma}{v_m}\right)^{-1.086} \tag{11}$$

$$c = \frac{v_m}{\Gamma(1+1/k)} \tag{12}$$

In addition, the energy pattern factor method (Weibull-EPM) is proposed. It is related to the mean values of the wind data, and the expressions are as follow:

$$\mathrm{E}_{pf} = \frac{\overline{v_m^3}}{v_m^3} \tag{13}$$

$$k = 1 + \frac{3.69}{\left(E_{pf}\right)^2} \tag{14}$$

$$c = \frac{v_m}{\Gamma(1+1/k)} \tag{15}$$

Where the E_{pf} is the energy pattern factor.

Moreover, some scholar proposed alternative maximum likelihood method (Weibull-AM), this method modifies the estimate of shape parameter.

$$k = \frac{\pi}{\sqrt{6}}\left[\frac{n(n-1)}{n(\sum_{i=1}^{n}\ln(v^2)) - (\sum_{i=1}^{n}\ln(v))^2}\right]^{1/2} \tag{16}$$

$$c = \left(\frac{1}{n}\sum_{i=1}^{n} v_i^k\right)^{1/k} \tag{17}$$

2.5. Evaluation of Weibull parameters

In order to check the suitable of Weibull distribution function for the measured data, three methods are proposed to examine the reliability of the data (see Table 3), the first is the root mean square error (RMSE), the second is the R-square, and the third is maximum absolute error (MAE) the expressions are defined as follows:

$$RMSE = \left[\frac{1}{n}\sum_{i=1}^{n}(y_i - x_i)^2\right]^{1/2} \tag{18}$$

$$R^2 = \frac{\sum_{i=1}^{n}(y_i - \bar{y})^2 - \sum_{i=1}^{n}(y_i - x_i)^2}{\sum_{i=1}^{n}(y_i - z_i)^2} \tag{19}$$

$$MAE = \frac{1}{n}\sum_{i=1}^{n}|y_i - x_i| \tag{20}$$

Where n is the number of observations, y_i is the frequency of the observations, x_i is the frequency obtained from the Weibull distribution, and $\bar{y}$ is the mean value of the observations.

2.6. Wind power density

Once the Weibull parameters are determined, the wind power density can be calculated by the related parameters. The wind power density can assess the wind energy potential at a certain site for wind turbine, and the evaluation expression can be obtained as follow (Jamil et al., 1995):

$$\frac{P}{A} = \frac{1}{2}\rho c^3\Gamma(1+\frac{3}{k}) \tag{21}$$

Where ρ is the density of air. The wind power density is related to the density of the air and to the cube of wind speed (Karthikeya et al., 2016). As we know, air density is sensitive to the temperature and atmospheric pressure which are related to the altitude. Therefore, the correction of air density should be considered when assessing wind energy potential (Fyrippis et al., 2010).

$$\rho = \rho_0\frac{T_0}{T}\left(1 - \frac{\gamma Z}{T_0}\right)^{\frac{g_0}{\gamma R}} \tag{22}$$

Where g_0 is the gravitational acceleration and equal to 9.81 $\mathrm{m/s^2}$, $R = 287$ $\mathrm{Jdeg^{-1}kg^{-1}}$ is gas constant, T is the atmospheric temperature in Kelvin, $T_0 = 288$ K, ρ_0 is the standard sea level air density and equal to 1.225 $\mathrm{kg/m^3}$, and γ is vertical temperature gradient, in this paper, set $\gamma = 6.5$ K/km as usual. In current investigation, the mean value of temperature in sample time is used as atmospheric temperature.

3. Results and discussion

3.1. Mean wind characteristics

Fig. 6 shows the mean wind characteristics, including wind speed and wind direction rose diagram based on all wind data, mean wind speed with error bar of standard deviation and its corresponding mean wind direction in different seasons, and diurnal mean wind speed profiles for four seasons, at six sites. As mentioned above, the series are split into spring, summer, autumn and winter, where spring is defined as March to May, summer as June through August, autumn as September through November, and winter as December to February. In general, the wind direction is uniform for the sites located in the valley, such as Baoshan site, Zanli site, Jin'an site and Yimen-C site, which agrees with the previous study (Belu and Koracin, 2013). When the sites are built in the flat area (Yimen-A site) or hilltop (Yimen-B site) in the mountainous areas, the wind direction is very chaotic, and the proportion of wind direction coming from all directions is not low, and this point is similar to wind characteristics in some coastal areas (Gualtieri and Secci, 2011; Oh et al., 2012). Overall, the higher the wind speed, the more concentrated the wind direction (Pérez et al., 2004). In order to better show the state of wind speed in different seasons, the seasonal mean wind speeds and mean wind directions are plotted, the error bar indicates the standard deviation of seasonal wind speed data. From the results, it is worth noting that although the four stations selected are separated by hundreds of kilometers, the mean wind speed in spring is always the largest, whereas the mean wind speed in summer is the smallest in the four seasons. Terrain can seriously affect wind direction and wind speed, so different regions have different wind characteristics(Cheynet et al., 2017; Huang et al., 2019; Mukut et al., 2008; Song et al., 2016; Wulfmeyer and Janjić, 2005). For the valleys where Zanli, Jin'an and Yimen are located, the mean wind direction varies little from season to season. Although Baoshan site is still located in the mountain area, its terrain is relatively flat, so the mean wind direction fluctuates greatly in different seasons, but the wind

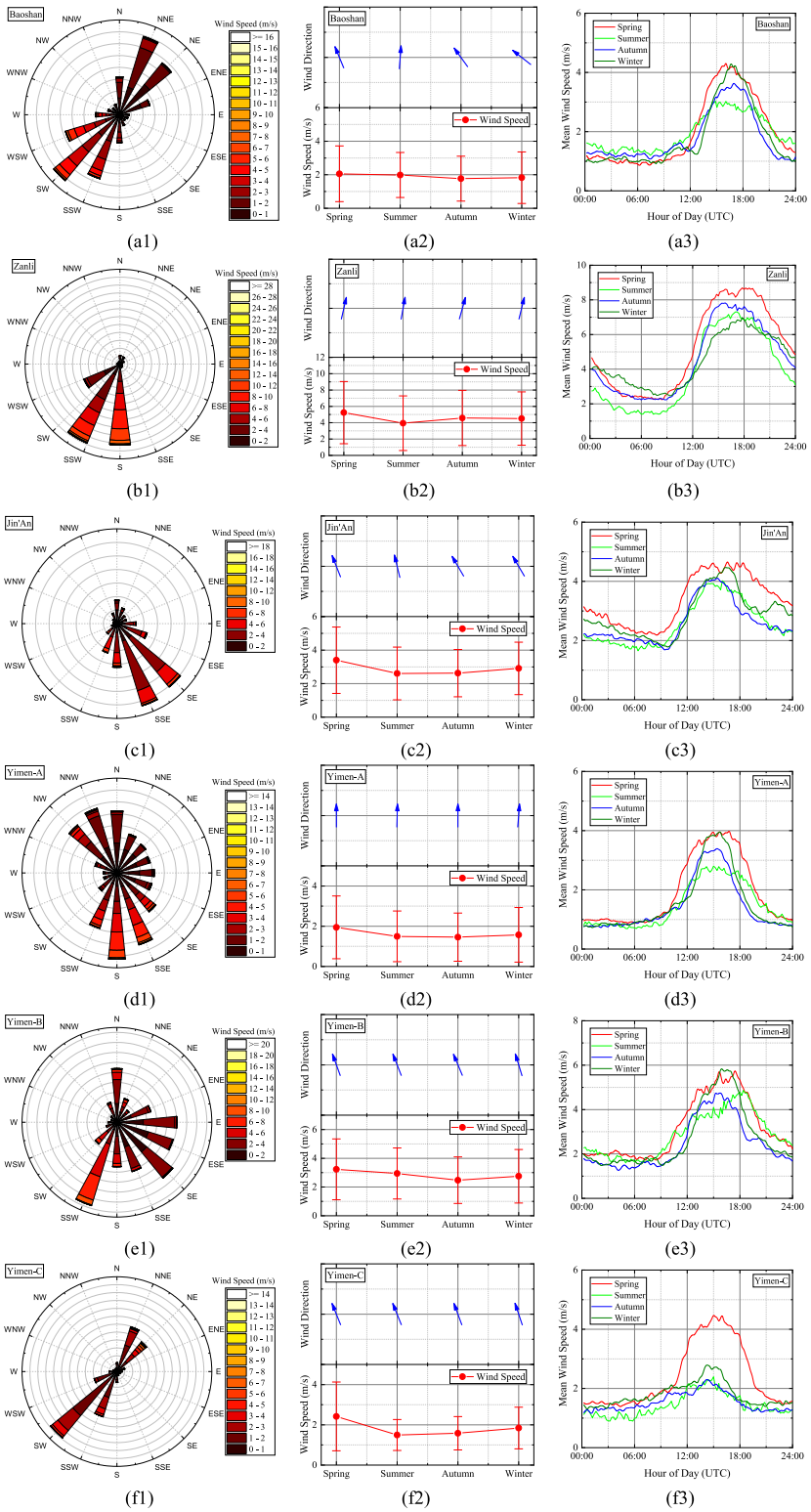

Fig. 6. Mean wind characteristics at (a) Baoshan site, (b) Zanli site, (c) Jin'an site, (d) Yimen-A site, (e) Yimen-B site and (f) Yimen-C site with (1) annual wind direction and wind speed distribution, (2) seasonal mean wind speed and wind direction, and (3) diurnal wind speed profiles.

direction generally remains as the south. It is also pointed out in some literatures that due to the influence of local topography, the wind direction in mountainous areas has a dominant direction (Zhang et al., 2020, 2019b). For diurnal wind speed profiles for six sites, mean wind speed is closely related to the rise and fall of the sun. The wind speed increases with the rise of the sun and reaches maximum value in the afternoon, and then the wind speed drops rapidly with the sunset. This is because the winds in the valley, also called valley winds, are usually caused by thermally induced pressure differences (Chow et al., 2013; Stewart et al., 2002; Tieleman, 2008). According to the change law of wind speed at night, there appears to be two types of profiles. One is that the wind speed rapidly decreases after the sun sets, and maintained at this wind speed with little fluctuation

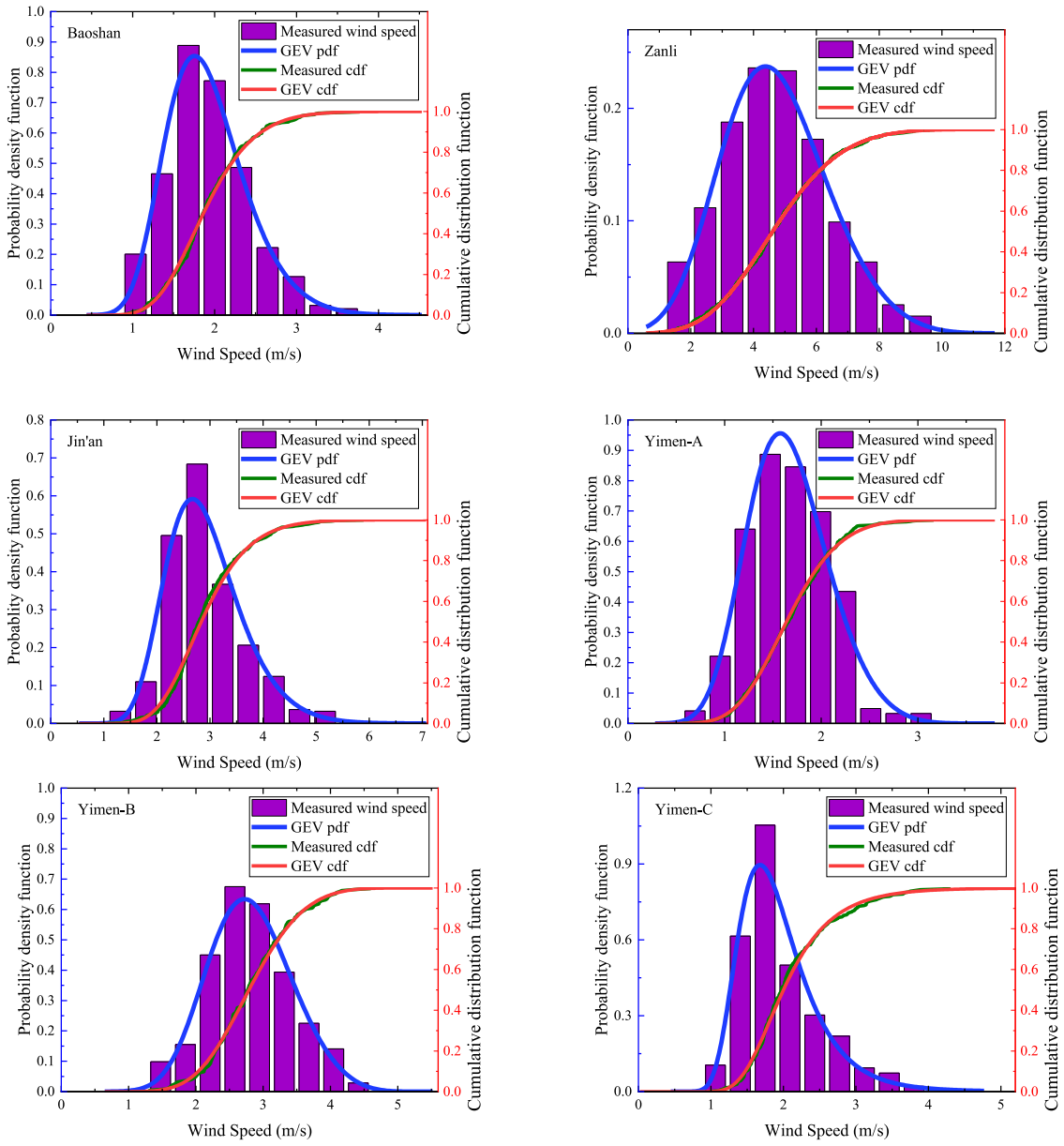

Fig. 7. Histogram of diurnal wind speeds observed at different sites.

until the sunrise of the next day. The measuring sites with this characteristic are Baoshan site and Yimen site. The other is that the wind speed slowly decreases after sunset, and the process can even last until the sunrise of the next day, such phenomenon can be found in Zanli site and Jin'an site. This phenomenon is related to the difference in altitude of the valley. It is well known that the temperature at the bottom of the valley is usually higher than that at the top of the mountain (Danielson et al., 2003; Kattel et al., 2013). As altitude difference of valley increases, the insulation effect is better, so the pressure difference caused by the thermal effect does not decrease immediately after the sunset, which makes the wind speed in the high-altitude difference area drop slower. In addition, the mean wind speed in different seasons also have significant differences, and the mean wind speed in spring is relatively large generally. In general, the mean wind speed in most areas of the mountain is smaller than the cut-in wind speed of modern wind turbines which is usually between 6 ∼10 m/s. Therefore, small wind turbines with low cut-in wind speed, such as AIRCON (small HAWT) or VAWTs (Dabiri, 2011) is recommended to equipped the distributed wind farm.

3.2. Return levels

Based on the daily mean wind speed, this section focuses on extreme value distribution characteristics of wind speeds of different stations and calculates the mean wind speed for different return period. Fig. 7 shows the theoretical probability density functions with the observed wind speed histograms for six sites. Also, the corresponding cumulative distribution functions are plotted in Fig. 7. In order to evaluate the correlation of fitting, three methods including R-square, root mean square error (RMSE) and mean absolute error (MAE) are introduced to examine the goodness of fit. Index of goodness and fitting parameters are listed in Table 1. In order of Baoshan, Zanli, Jin'an, Yimen-A, Yimen-B and Yimen-C, the shape parameters are −0.1076, −0.1935, −0.0903, −0.1750, −0.2201 and 0.0416, respectively, the scale parameters are 0.4335, 1.5813, 0.6245, 0.3911, 0.5955 and 0.4111, respectively, the location parameters are 1.7065, 4.0448, 2.6092, 1.5011, 2.5784 and 1.6937, respectively in the corresponding site.

Table 1
Summary of GEV parameters and correlation of fit at six sites.

Site	GEV Parameters			Goodness of fit		
	ξ	α	μ	R-Square	RMSE	MAE
Baoshan	−0.1076	0.4335	1.7065	0.9978	0.0137	0.0104
Zanli	−0.1935	1.5813	4.0448	0.9992	0.0080	0.0062
Jin'an	−0.0903	0.6245	2.6092	0.9931	0.0239	0.0205
Yimen-A	−0.1750	0.3911	1.5011	0.9988	0.0099	0.0078
Yimen-B	−0.2201	0.5955	2.5784	0.9979	0.0131	0.0107
Yimen-C	0.0416	0.4111	1.6937	0.9958	0.0187	0.0157

According to the values of R-Square, RMSE and MAE, the GEV distribution performs well for the total of six sites. The values of R-Square, RMSE and MAE are 0.9978, 0.0137 and 0.0104 in Baoshan, 0.9992, 0.0080 and 0.0062 in Zanli, 0.9931, 0.0239 and 0.0205 in Jin'an, around 0.9979, 0.0131 and 0.107 in Yimen. As mentioned in Section 2.3, the shape parameter is very important. For a total of five sites, the shape parameter is negative, indicating a bound distribution, which that it is theoretically impossible for the mean wind speed of the site to be above the upper bound of the corresponding site (Castillo, 1988; Kruyt et al., 2017). Therefore, for such dry–hot valleys affected by monsoon season, the extreme value distribution is more in accordance with Frechet distribution, also called Extreme distribution Type II. Ayuketang Arreyndip and Joseph took west coast area of Africa as an example, and the applicability of different extreme value distribution models was compared. The results showed that Frechet distribution had better coincidence (Ayuketang Arreyndip and Joseph, 2016). Also, similar cases were found in South America (de Oliveira et al., 2011). Based on the results of extreme value distribution, the mean wind speed with a return period of 5 years and 10 years at 10 m high above the ground are given and listed in Table 2. The predicted mean wind speed with return period of 10 years is 4.07 m/s in Baoshan site, 10.54 m/s in Zanli site, 6.24 m/s in Jin'an site, 3.21 m/s in Yimen-A site, 4.85 m/s in Yimen-Bsite and 5.72 m/s in Yimen-C site. For the three sites of Yimen, supposed that the climatic conditions of the three sites are the same for the close distance because the adjacent site. Observe the predicted mean wind speed of the three sites, the difference is very large. The site located in the valley (Yimen-C) has the largest mean wind speed while the site on the flat terrain (Yimen-A) has the smallest. This is because wind characteristics in mountainous areas are significantly affected by the terrain. When the site is in the valley, wind is constrained by the mountain, causing the wind speed and wind direction to be relatively concentrated, so it is accompanied by a higher wind speed. For flat areas in mountainous areas surrounded by mountains, the wind is blocked by the surrounding mountains, so the wind speed is low and the wind direction is disordered. Compare four different places, although these four places are located in mountainous areas, the wind speed with same return period is quite different. For the return period of 5 years, the minimum wind speed is 3.133 m/s at Yimen-A site, the maximum wind speed is 10.301 m/s in Zanli site. For the return period of 10 years, the sites of the maximum and minimum wind speeds are the same as the return period of 5 years. It can be seen that the influence of local topography on wind environment is enormous. There is perennial snow on the top of the mountain around the Zanli site, which leads to a greater temperature difference, resulting in a large wind speed. Contrarily, the temperature in Yimen site is relatively warm, so the wind speed is relatively low. As the return period increases, the wind speed increases slightly, which is consistent with the trend of CDF.

3.3. Weibull distribution

Fig. 8 depicts the Weibull distribution to wind speed histograms of all wind speed data with five estimate methods, and statistical parameters with three types of goodness of fit criteria at different sites are tabulated in Tables 3–8. As Fig. 8 showed, all methods fit the observed data well except for Weibull-AM (Alternative Maximum Likelihood Method). The performance of Weibull-AM is not stable. For Zanli and Yimen-C, the estimation values are close to those of other four methods, while for the other four sites, the estimation values are much larger or smaller, and the maximum deviation can even reach 30%. Therefore, the following discussion mainly focus on other four methods. The shape parameters (k) are derived from the well-fit methods are centered with the values around 1.32 at Baoshan site, 1.41 at Zanli site, 1.82 at Jin'an site, 1.37 at Yimen-A site, 1.60 at Yimen-B site, 1.52 at Yimen-C site, whereas the scale parameters (c) determined from the corresponding sites are with an average value of 2.08, 5.31, 3.30, 2.11, 3.21, 2.17, respectively. As found, the highest value of RMSE is calculated by Alternative Maximum Likelihood method, 0.08899, occurred at Baoshan site. The corresponding R-Square is also the smallest, with a value of 0.9050. For the three sites in Yimen, Weibull parameters are different as well. Compared with coastal open area, the values of Weibull parameters are much smaller, especially for the scale parameters. In Taiwan, the Weibull parameters in Dayuan, Hengchun and Penghu are estimated, the scale parameters are between 8.5 to 11 which is much larger than those in this paper, while the shape parameters are relatively close to those in this paper (Chang, 2011). For the urban area, the results are much closer. Taking Singapore as an example, the Weibull parameters at the roof of tall building in urban were estimated (Karthikeya et al., 2016).

Energy consumption is unevenly distributed over time. Therefore, it is necessary to explore the Weibull parameters in different seasons. The Weibull parameters obtained from spring, summer, autumn and winter at six sites are listed in Table 9. Generally, the shape parameters in summer is larger than that in other seasons, whereas the corresponding scale parameters are smaller. For different seasons and measuring sites, the Weibull parameters calculated by different methods are very close except for Weibull-AM.

3.4. Wind energy assessment

According to Eq. (21), the wind power density can be obtained by Weibull shape parameter and Weibull scale parameter. Accurate assessment of wind power density can improve the economy and applicability of wind turbines. Table 10 summarizes the calculated wind power density at all measurement sites with different estimate methods. In order to compare the influence of air density, the data in parentheses is calculated with the air density which is not corrected with altitude and temperature. As found, except Weibull-AM, the wind power densities estimated by the other four methods are close to each other. In addition, comparing the wind power density of different sites, the difference of wind power density is huge. The wind power density at

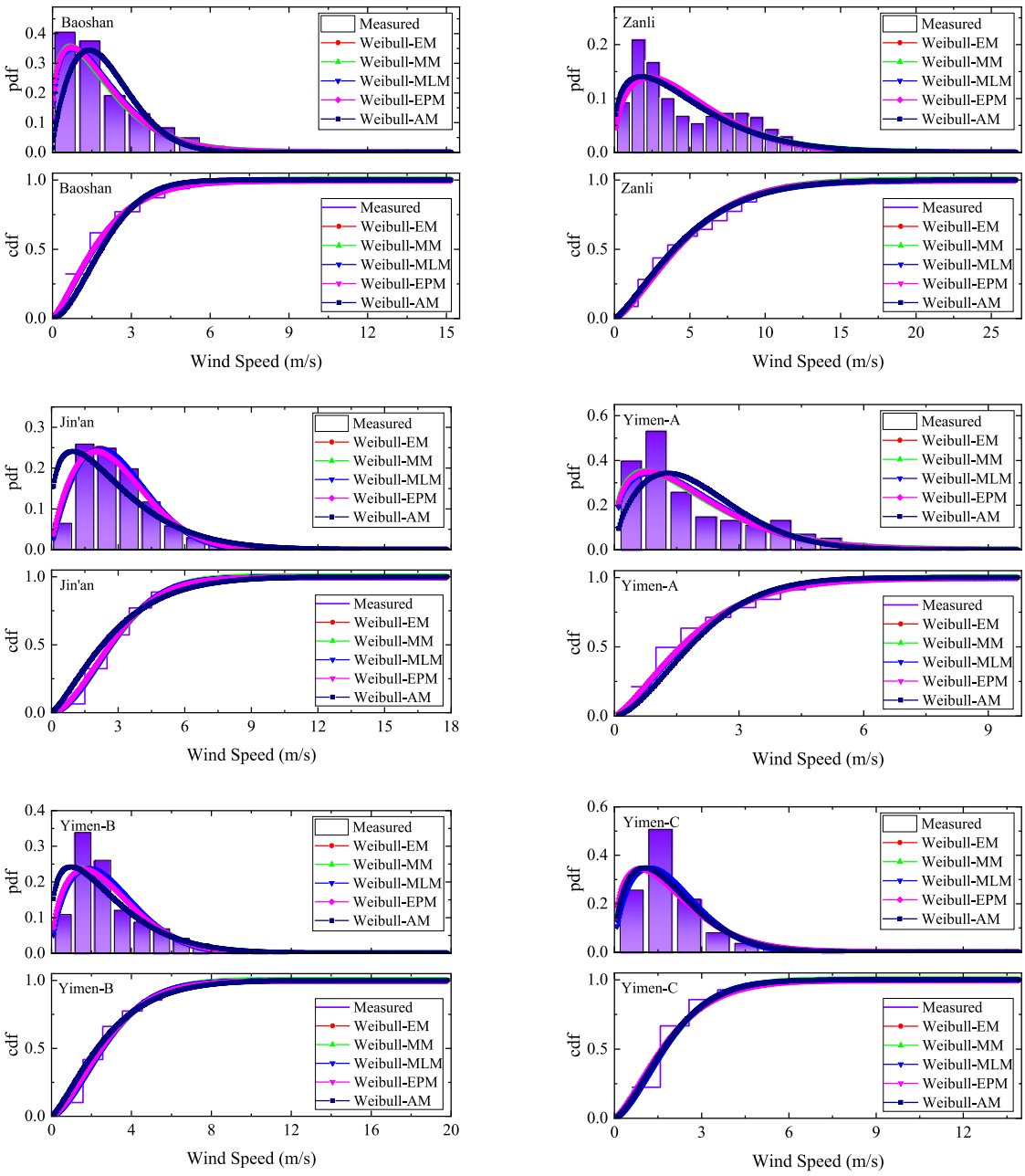

Fig. 8. Weibull distribution for wind speeds at different sites, five estimate methods compared.

Table 2
Mean wind speed at different sites with different return period.

Return period (years)	Mean wind speed (m/s)					
	Baoshan	Zanli	Jin'an	Yimen-A	Yimen-B	Yimen-C
5	3.935	10.301	6.007	3.133	4.758	5.301
10	4.070	10.541	6.237	3.208	4.850	5.719

Table 3
Statistical parameters of all wind speed data with five estimate methods (Baoshan site).

Estimate method	Weibull parameters		Goodness of fit		
	k	*c*	R-Square	RMSE	MAE
Weibull-EM	1.322	2.078	0.9932	0.02379	0.02064
Weibull-MM	1.297	2.070	0.9940	0.02228	0.01945
Weibull-MLM	1.343	2.093	0.9917	0.02635	0.02236
Weibull-EPM	1.317	2.076	0.9934	0.02345	0.02039
Weibull-AM	1.735	2.292	0.9050	0.08899	0.07489

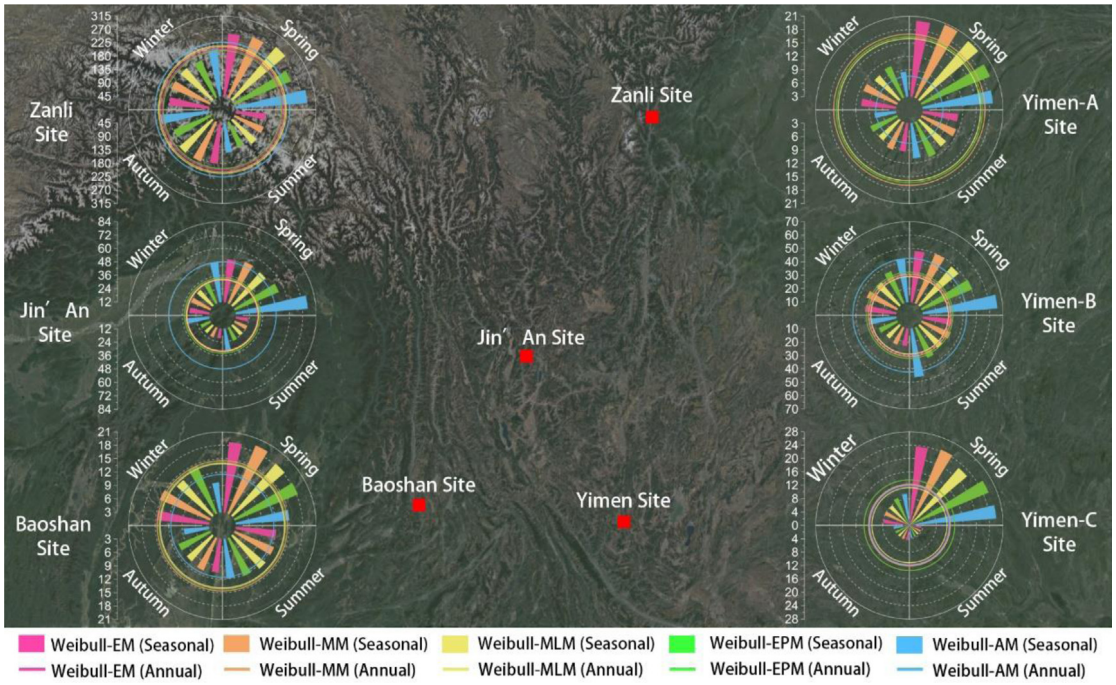

Fig. 9. Seasonal wind power density with different estimate methods at six sites.

Table 4
Statistical parameters of all wind speed data with five estimate methods (Zanli site).

Estimate method	Weibull parameters		Goodness of fit		
	k	*c*	R-Square	RMSE	MAE
Weibull-EM	1.423	5.312	0.9755	0.04516	0.03798
Weibull-MM	1.393	5.295	0.9789	0.04192	0.03545
Weibull-MLM	1.378	5.292	0.9804	0.04041	0.03429
Weibull-EPM	1.444	5.323	0.9730	0.04746	0.03983
Weibull-AM	1.323	5.227	0.9847	0.03567	0.03069

Table 5
Statistical parameters of all wind speed data with five estimate methods (Jin'an site).

Estimate method	Weibull parameters		Goodness of fit		
	k	*c*	R-Square	RMSE	MAE
Weibull-EM	1.855	3.300	0.9966	0.01687	0.01444
Weibull-MM	1.808	3.296	0.9962	0.01776	0.01468
Weibull-MLM	1.854	3.312	0.9961	0.01809	0.01571
Weibull-EPM	1.745	3.290	0.9948	0.02090	0.01700
Weibull-AM	1.288	3.059	0.9190	0.08217	0.06958

Table 6
Statistical parameters of all wind speed data with five estimate methods (Yimen-A site).

Estimate method	Weibull parameters		Goodness of fit		
	k	*c*	R-Square	RMSE	MAE
Weibull-EM	1.363	2.104	0.9718	0.04850	0.04156
Weibull-MM	1.336	2.097	0.9739	0.04664	0.04007
Weibull-MLM	1.400	2.127	0.9669	0.05249	0.04429
Weibull-EPM	1.363	2.104	0.9718	0.04852	0.04158
Weibull-AM	1.656	2.252	0.9060	0.08851	0.07112

Table 7
Statistical parameters of all wind speed data with five estimate methods (Yimen-B site).

Estimate method	Weibull parameters		Goodness of fit		
	k	*c*	R-Square	RMSE	MAE
Weibull-EM	1.623	3.216	0.9804	0.04037	0.03404
Weibull-MM	1.583	3.208	0.9808	0.04002	0.03357
Weibull-MLM	1.659	3.241	0.9781	0.04272	0.03562
Weibull-EPM	1.546	3.201	0.9805	0.04035	0.03354
Weibull-AM	1.296	3.041	0.9529	0.06263	0.04604

Table 8
Statistical parameters of all wind speed data with five estimate methods (Yimen-C site).

Estimate method	Weibull parameters		Goodness of fit		
	k	*c*	R-Square	RMSE	MAE
Weibull-EM	1.539	2.167	0.9668	0.05259	0.04593
Weibull-MM	1.503	2.162	0.9641	0.05469	0.04753
Weibull-MLM	1.623	2.196	0.9686	0.05113	0.04471
Weibull-EPM	1.404	2.141	0.9528	0.06270	0.05350
Weibull-AM	1.505	2.147	0.9650	0.05399	0.04665

Table 9
Summarization of Weibull parameters at six stations in different seasons and estimate methods.

Site	Season	Weibull-EM		Weibull-MM		Weibull-MLM		Weibull-EPM		Weibull-AM	
		k	*c*	*k*	*c*	*k*	*c*	*k*	*c*	*k*	*c*
Baoshan	Spring	1.269	2.215	1.247	2.207	1.297	2.236	1.288	2.223	1.631	2.434
	Summer	1.542	2.205	1.505	2.198	1.492	2.196	1.527	2.202	1.610	2.244
	Autumn	1.359	1.927	1.332	1.920	1.368	1.936	1.348	1.925	1.931	2.186
	Winter	1.207	1.942	1.190	1.934	1.281	1.981	1.221	1.947	1.882	2.230
Zanli	Spring	1.474	5.893	1.441	5.875	1.399	5.845	1.499	5.905	1.365	5.804
	Summer	1.263	4.393	1.241	4.376	1.244	4.389	1.309	4.426	1.283	4.437
	Autumn	1.450	5.196	1.418	5.179	1.414	5.187	1.475	5.207	1.321	5.084
	Winter	1.472	5.170	1.439	5.154	1.448	5.169	1.470	5.169	1.324	5.037
Jin'an	Spring	1.837	3.855	1.790	3.850	1.842	3.871	1.721	3.842	1.285	3.576
	Summer	1.773	2.948	1.728	2.944	1.773	2.959	1.698	2.941	1.316	2.763
	Autumn	2.026	2.968	1.974	2.967	2.007	2.978	1.953	2.966	1.305	2.738
	Winter	1.987	3.310	1.936	3.308	1.968	3.319	1.890	3.305	1.286	3.049
Yimen-A	Spring	1.385	2.424	1.357	2.415	1.385	2.435	1.405	2.429	1.494	2.495
	Summer	1.540	2.134	1.504	2.128	1.578	2.154	1.496	2.127	1.566	2.149
	Autumn	1.387	1.881	1.358	1.874	1.437	1.905	1.375	1.878	1.873	2.088
	Winter	1.299	1.866	1.276	1.859	1.355	1.894	1.309	1.868	1.958	2.177
Yimen-B	Spring	1.643	3.613	1.602	3.605	1.669	3.639	1.580	3.600	1.283	3.405
	Summer	1.751	3.269	1.706	3.263	1.769	3.287	1.662	3.257	1.291	3.053
	Autumn	1.674	2.842	1.632	2.837	1.702	2.861	1.587	2.830	1.329	2.689
	Winter	1.576	3.098	1.538	3.090	1.623	3.127	1.503	3.082	1.305	2.950
Yimen-C	Spring	1.477	2.679	1.444	2.671	1.550	2.716	1.405	2.66	1.361	2.614
	Summer	2.075	1.678	2.022	1.678	2.043	1.682	1.956	1.676	1.912	1.657
	Autumn	2.052	1.778	2.000	1.778	2.019	1.781	1.939	1.776	1.771	1.732
	Winter	1.897	2.084	1.848	2.082	1.900	2.091	1.701	2.073	1.508	1.982

Zanli site is around 210 W/m^2, which is almost 18 times that of Yimen-A and Yimen-C sites. Clearly, the wind power density associated with hilltop are higher than that in valley and on flat terrain. Despite the wind power density reaches 210 W/m^2, the wind energy density in mountainous areas is still relatively low. Moreover, the estimated wind power density will be larger if the unmodified air density is used, but the effect is limited, and the error caused by the unmodified air density is generally controlled within 2%.

But it is worth noting that the electricity consumption is different in each season, for example, due to heating and cooling demand, electricity consumption in winter and summer will increase significantly (Xia et al., 2014). Similarly, according to previous research results, wind energy density also shows a certain seasonality (Kruyt et al., 2017). Hence to assess the wind power density in different seasons, according to the Weibull parameters listed in Table 9, the wind power densities of different sites are also calculated and shown in Fig. 9. As can be found, whichever measuring site and estimate method are adopted, the wind power density in spring is the largest, followed by winter. Carneiro et al. pointed that the wind energy density is Brazil has the same trend, the power density reaches maximum in Spring (Carneiro et al., 2016). Compared to the other four sites, the wind power densities of Zanli site and Banshan site are relatively balanced in different seasons. Analyzing the three sites at Yimen, the hilltop or the valley is better for the location of small distributed wind farm in mountainous area, because the wind energy obtained is the most impressive. At the same time, small wind turbines with low starting wind speed should be selected as the power source. Also, it is necessary to avoid building wind turbines in the flat land surrounded by mountains as far as possible.

3.5. Sociality and economy

Economic and social effects are an integral part. In the area of sociality, the buffer zones should be considered. Construction work, such as building dams, bridges, etc. does have an impact on the environment, changes in the environment will not only affect animals and plants in nature, but also humans themselves. In order to minimize the impact of wind farms on humans and the natural environment, many aspects of buffer zones, such as protected areas (including bird area, natural park, natural conversion area, etc.), water bodies (river, lake, well, etc.), settlements, production land, road, etc. For the research object in this manuscript, due to the undulating geographic environment of the mountain areas, the value and density of the population are much lower than those of the cities, and the available land resources are relatively limited, so the buffer zones of water bodies, settlements and road could set to 200 m, 500 m, and 200 m, respectively, while the buffer zone of protection areas should be set to a value larger than 500 m (Ayodele et al., 2018; Barakat et al., 2017; Enevoldsen and Permien, 2018; Mahdy and Bahaj, 2018).

In the aspect of economy, taking a family of 3 persons as an example, each home is designed with a rated power of 3 kW. This power can meet the daily use of the family and effectively load household appliances such as TV, desktop, refrigerator, washing machine, microwave, etc. Thus, the wind turbine with rated power of 10 kW is selected. In order to ensure the normal power

Table 10
Comparison of wind power density with various Weibull parameters at six sites.

Site	Power density (W/m^2)				
	Weibull-EM	Weibull-MM	Weibull-MLM	Weibull-EPM	Weibull-AM
Baoshan	14.10 (14.29)	14.58 (14.78)	13.90 (14.08)	14.19 (13.90)	11.51 (11.66)
Zanli	202.27 (203.36)	209.39 (210.52)	213.92 (215.07)	197.64 (198.70)	225.80 (227.02)
Jin'an	31.59 (31.88)	32.51 (32.81)	31.96 (32.25)	33.90 (34.21)	48.05 (48.50)
Yimen-A	10.79 (10.95)	11.14 (11.30)	9.92 (10.06)	10.70 (10.85)	6.27 (6.37)
Yimen-B	35.04 (35.59)	36.22 (36.79)	34.66 (35.20)	37.47 (38.06)	46.21 (46.94)
Yimen-C	11.74 (11.90)	12.16 (12.33)	11.17 (11.33)	13.50 (13.69)	11.88 (12.05)

Note: The data in parentheses are calculated using air density at standard sea level.

supply of a family, a distributed DWES of a family should contain an inverter, a controller, a battery, cables and a wind turbine. The entire system is uniformly controlled by the controller. The wind generator generates electricity, and the excess electricity will be stored in the battery. When the wind is reduced and the electricity generated by the wind generator is insufficient, the inverter will supplement electrical energy from the battery.

The total cost of a DWES for a family is composed of capital cost and operation and maintenance cost. The capital cost consists of wind power equipment cost and other expenses related to civil works and material cost. The total cost of 1kWh wind-generated electricity is as followed (Saeidi et al., 2013):

$$C = \underbrace{\frac{C_I}{8760n} \cdot \left(\frac{1}{P_R \cdot CF}\right)}_{capital\ cost} + \underbrace{\frac{C_I}{8760n} \cdot \left(\frac{1}{P_R \cdot CF}\right) \cdot m \cdot \left(\frac{(1+I)^n - 1}{I(1+I)^n}\right)}_{operation\ and\ maintenance\ cost} \tag{23}$$

Where, C_I is the total investment, n is the useful life of the DWES, P_R is the rated power of wind turbine, CF is the capacity factor which can be assumed as 21.3 (IEA, 2018), m is the percentage that determines the annual cost of operation and maintenance of the DWES, I is the annual interest rate.

Unlike Europe and other countries, the operation and maintenance costs of power system are not calculated based on a percentage of total cost, but are calculated based on per kilowatt-hour (kWh). Therefore, the calculation items related to operation and maintenance costs in the formula are not considered for the time being, and only the equipment costs and installation costs are calculated. For the small wind turbine, usually VAWTs and HAWTs can be selected. The price of a set of a distributed wind energy system with VAWT is about CNY 65,000, while the price is CNY 45,000 with HAWT. Other initial costs including installation, transportation, and custom fee is assumed about 40% of the system (Saeidi et al., 2013). Useful life of the system is 15 years. In addition, we assume that the average operational and maintenance cost of the distributed wind farm is set as 0.10 CNY/kWh (Tu et al., 2019). Thus, the price with VAWTs is about 0.406 CNY/kWh, the price with HAWTs is 0.305 CNY/kWh. And the market electricity price of China is around 0.56 CNY/kWh which is depended on the location (Qiu and Anadon, 2012; Rodrigues et al., 2017).

4. Concluding remarks

Wind energy is a clean and highly valuable renewable energy. With the development of wind energy technology, it has gradually become an important branch of energy technology. By means of measurement method, the wind characteristics at six sites in different seasons and different times of the day in complex mountainous areas are investigated. Energy estimated methods and potential assessment for distributed wind farm are carried out.

Accurate estimation of wind characteristics is the basis of wind energy potential assessment. Generally, affected by the topography, the wind direction in the valley has directivity, while the wind direction in the flat terrain surround by mountains is chaotic. Wind speed is greatly affected by season. The maximum wind speed occurs in spring, while the minimum wind speed occurs in summer. In addition, the mean wind direction seems to be season-independent. Driven by thermal effect, the diurnal wind speed is related to the spatial position of the sun and increases with a peak in the afternoon.

With negative shape parameter, wind data in mountainous areas are more in line with Frechet distribution, also called Extreme distribution Type II. Among measurement data from six sites, the mean wind speeds for 5-year and 10-year return periods range from 3.133 to 10.301 m/s and from 3.208 to 10.541 m/s, respectively. The maximum wind speed with different return period occurs in deep-cut canyon surrounded by mountains covered with snow all the year round (Zanli site), while the minimum occurs in flat terrain surrounded by mountains (Yimen-A site).

For energy application, Weibull parameters and estimated energy potential are calculated with five methods. In addition to alternative maximum likelihood method, the other four methods, namely empirical method, moment method, maximum likelihood method and energy pattern factor method, are highly applicable to mountain environments. Thus, estimation methods suitable for coastal areas can also be used for energy assessment in mountain environments. Wind energy potential affect by climate and topography significant, the wind power density in Zanli is over 200 W/m^2, while the power density in Yimen-A is less than 10 W/m^2. Similar to mean wind characteristics, wind power density shows strong seasonality, with the maximum value in spring and the lowest value in summer. For wind power facilities built in complex mountainous areas, power generation facilities should be built in valleys or on the top of the mountain, and should not be built in the flat land surrounded by mountains. National policies are crucial for energy development. For the remote mountainous areas mentioned in this paper, the development of distributed wind power system is one of the ways to solve the power shortage in such areas.

For the sociality and economy. A buffer zone should be set to minimize the impact of wind farm on natural environment. Also, the total cost of 1kWh wind-generated electricity is calculated, the cost of a DWES with VAWTs and a DWES with HAWTs is 0.406 CNY/kWh and 0.305 CNY/kWh, respectively.

In addition, the stability of the power system is very important. In the subsequent research, robustness research will be carried out for the DWES system.

Nomenclature

See Table 11.

Table 11

List of symbols	
$g(x)$	Probability density function of GEV distribution
$G(x)$	Cumulative distribution function of GEV distribution
μ	Location parameter of GEV distribution
α	Scale parameter of GEV distribution (m/s)
ξ	Shape parameter of GEV distribution
P_0	Return period (yr.)
$w(x)$	Probability density function of Weibull distribution
$W(x)$	Cumulative distribution function of Weibull distribution
k	Shape parameter of Weibull distribution
c	Scale parameter of Weibull distribution (m/s)
v_m	Mean wind speed of wind sample (m/s)
σ	Standard deviation of the wind speed sample (m/s)
$\Gamma()$	Gamma function
E_{pf}	Energy pattern factor
$RMSE$	Root mean square error
R^2	Coefficient of determination
MAE	Maximum absolute error
P/A	Power density (W/m^2)
ρ	Density of air (kg/m^3)
ρ_0	Standard sea level air density (equal to 1.225 kg/m^3)
T	Atmospheric temperature in Kelvin (K)
T_0	15 Celsius degrees in Kelvin (equal to 288 K)
g_0	Gravitational acceleration (equal to 9.81 m/s^2)
R	Gas constant (equal to 287 $Jdeg^{-1}kg^{-1}$)
γ	Vertical temperature gradient (equal to 6.5 K/km)
C	Total cost of 1 kWh wind-generated electricity
C_I	Total investment including capital cost and operation and maintenance cost
n	Useful life of the DWES (year)
P_R	Rated power of wind turbine (kW)
CF	Capacity factor
m	Ratio of operation and maintenance cost to the cost of DWES
I	Interest rate

Declaration of competing interest

The authors declare that they have no known competing financial interests or personal relationships that could have appeared to influence the work reported in this paper.

CRediT authorship contribution statement

Mingjin Zhang provide the data, give some advices on this article and give the funding support. Jingyu Zhang analyzed, visualized, wrote the manuscript and wrote the analysis code. Yongle Li gave many meaningful guidance on the wind tunnel tests, analysis and writing of this paper. Jiaxin Yu worked on the article revisions. Jingxi Qing worked together on the article revisions. Kai Wei worked together on the data analysis. Lili Song provided some measured data.

Acknowledgments

The work described in this paper was fully supported by a grant from the National Key R&D Program of China (No. 2018YFC1507800), grants from the National Natural Science Foundation of China (nos. 51525804, 51708464), a grant from the Hunan Provincial Transportation Science and Technology Project (No. 201615) and a grant from the Fundamental Research Funds for the Central Universities (No. 2682019CX02).

References

Allan, G., Eromenko, I., Gilmartin, M., Kockar, I., McGregor, P., 2015. The economics of distributed energy generation: A literature review. Renew. Sustain. Energy Rev. 42, 543–556.

Ayodele, T.R., Ogunjuyigbe, A.S.O., Odigie, O., Munda, J.L., 2018. A multi-criteria GIS based model for wind farm site selection using interval type-2 fuzzy analytic hierarchy process: The case study of Nigeria. Appl. Energy 228, 1853–1869.

Ayuketang Arreyndip, N., Joseph, E., 2016. Generalized extreme value distribution models for the assessment of seasonal wind energy potential of debuncha. Cameroon. J. Renew. Energy 2016, 935781.

Barakat, A., Hilali, A., Baghdadi, M.E., Touhami, F., 2017. Landfill site selection with GIS-based multi-criteria evaluation technique. A case study in Béni Mellal-Khouribga region. Morocco. Environ. Earth Sci. 76 (413).

Bayod-Rújula, A.A., 2009. Future development of the electricity systems with distributed generation. Energy 34, 377–383, WESC 2006.

Belu, R., Koracin, D., 2013. Statistical and spectral analysis of wind characteristics relevant to wind energy assessment using tower measurements in complex terrain. J. Wind Energy 2013, 1–12.

Carneiro, T.C., Melo, S.P., Carvalho, P.C.M., Braga, A.P. de S., 2016. Particle swarm optimization method for estimation of Weibull parameters: A case study for the Brazilian northeast region. Renew. Energy 86, 751–759.

Castillo, E., 1988. Extreme Value Theory in Engineering. In: Statistical Modeling and Decision Science, Academic Press.

Chang, T.P., 2011. Performance comparison of six numerical methods in estimating Weibull parameters for wind energy application. Appl. Energy 88, 272–282.

Chaurasiya, P.K., Ahmed, S., Warudkar, V., 2018. Comparative analysis of Weibull parameters for wind data measured from met-mast and remote sensing techniques. Renew. Energy 115, 1153–1165.

Cheynet, E., Jakobsen, J.B., Obhrai, C., 2017. Spectral characteristics of surface-layer turbulence in the North Sea. In: Energy Procedia, 14th Deep Sea Offshore Wind R & D Conference, EERA DeepWind'2017, vol. 137, pp. 414–427.

Chong, W.T., Naghavi, M.S., Poh, S.C., Mahlia, T.M.I., Pan, K.C., 2011. Techno-economic analysis of a wind–solar hybrid renewable energy system with rainwater collection feature for urban high-rise application. Appl. Energy 88, 4067–4077.

Chong, W.T., Pan, K.C., Poh, S.C., Fazlizan, A., Oon, C.S., Badarudin, A., Nik-Ghazali, N., 2013. Performance investigation of a power augmented vertical axis wind turbine for urban high-rise application. Renew. Energy 51, 388–397.

Chow, F.K., Wekker, S.F.J.D., Snyder, B.J. (Eds.), 2013. Mountain Weather Research and Forecasting: Recent Progress and Current Challenges. Springer Atmospheric Sciences, Springer Netherlands.

Cost Rocha, P.A., de Sousa, R.C., de Andrade, C.F., da Silva, M.E.V., 2012. Comparison of seven numerical methods for determining Weibull parameters for wind energy generation in the northeast region of Brazil. Appl. Energy 89, 395–400 (Special issue on Thermal Energy Management in the Process Industries).

Dabiri, J.O., 2011. Potential order-of-magnitude enhancement of wind farm power density via counter-rotating vertical-axis wind turbine arrays. J. Renew. Sustain. Energy 3, 043104.
Danielson, E.W., Levin, J., Abrams, E., 2003. Meteorology. McGraw-Hill.
Enevoldsen, P., Permien, F.-H., 2018. Mapping the wind energy potential of sweden: A sociotechnical wind atlas. J. Renew. Energy 2018, 1650794.
Fisher, R.A., 1915. Frequency distribution of the values of the correlation coefficient in samples from an indefinitely large population. Biometrika 10, 507–521.
Fyrippis, I., Axaopoulos, P.J., Panayiotou, G., 2010. Wind energy potential assessment in Naxos island. Greece. Appl. Energy 87, 577–586.
Global Wind Energy Council, 2019. Global wind report. Annual Market Update 2018.
Gualtieri, G., Secci, S., 2011. Wind shear coefficients, roughness length and energy yield over coastal locations in Southern Italy. Renew. Energy 36, 1081–1094.
Huang, G., Jiang, Y., Peng, L., Solari, G., Liao, H., Li, M., 2019. Characteristics of intense winds in mountain area based on field measurement: Focusing on thunderstorm winds. J. Wind Eng. Ind. Aerodyn. 190, 166–182.
IEA, 2018. IEA Wind TCP 2017 Annual Report. International Energy Agency.
Jamil, M., Parsa, S., Majidi, M., 1995. Wind power statistics and an evaluation of wind energy density. Renew. Energy Solar Electr. Photovoltaics Wind 6, 623–628.
Jenkinson, A.F., 1955. The frequency distribution of the annual maximum (or minimum) values of meteorological elements. Q. J. R. Meteorol. Soc. 81, 158–171.
Jiang, Y., Zhao, N., Peng, L., Liu, S., 2019. A new hybrid framework for probabilistic wind speed prediction using deep feature selection and multi-error modification. Energy Convers. Manag. 199, 111981.
Justus, C.G., Mikhail, A., 1976. Height variation of wind speed and wind distributions statistics. Geophys. Res. Lett. 3, 261–264.
Karthikeya, B.R., Negi, P.S., Srikanth, N., 2016. Wind resource assessment for urban renewable energy application in Singapore. Renew. Energy 87, 403–414.
Kattel, D.B., Yao, T., Yang, K., Tian, L., Yang, G., Joswiak, D., 2013. Temperature lapse rate in complex mountain terrain on the southern slope of the central Himalayas. Theor. Appl. Climatol. 113, 671–682.
Kaundinya, D.P., Balachandra, P., Ravindranath, N.H., 2009. Grid-connected versus stand-alone energy systems for decentralized power—A review of literature. Renew. Sustain. Energy Rev. 13, 2041–2050.
Khan, K.S., Tariq, M., 2018. Wind resource assessment using SODAR and meteorological mast – A case study of Pakistan. Renew. Sustain. Energy Rev. 81, 2443–2449.
Khare, V., Nema, S., Baredar, P., 2016. Solar–wind hybrid renewable energy system: A review. Renew. Sustain. Energy Rev. 58, 23–33.
Köse, R., 2004. An evaluation of wind energy potential as a power generation source in Kütahya. Turk. Energy Convers. Manag. 45, 1631–1641.
Kose, R., Ozgur, M.A., Erbas, O., Tugcu, A., 2004. The analysis of wind data and wind energy potential in Kutahya. Turkey. Renew. Sustain. Energy Rev. 8, 277–288.
Kristensen, L., 1998. Cup anemometer behavior in turbulent environments. J. Atmos. Ocean. Technol. 15, 5–17.
Kristensen, L., 1999. The perennial cup anemometer. Wind Energy 2, 59–75.
Kruyt, B., Lehning, M., Kahl, A., 2017. Potential contributions of wind power to a stable and highly renewable Swiss power supply. Appl. Energy 192, 1–11.
Kumar, R., Raahemifar, K., Fung, A.S., 2018. A critical review of vertical axis wind turbines for urban applications. Renew. Sustain. Energy Rev. 89, 281–291.
Lee, J.K., Yook, D., Lee, K.J., Yun, J.-I., Beeley, P.A., 2015. Weibull parameter calculation and estimation of directional and seasonal wind speeds for the return period: A case study in the barakah NPP area. Ann. Nucl. Energy 80, 62–69.
Lu, L., Ip, K.Y., 2009. Investigation on the feasibility and enhancement methods of wind power utilization in high-rise buildings of Hong Kong. Renew. Sustain. Energy Rev. 13, 450–461.
Mahdy, M., Bahaj, A.S., 2018. Multi criteria decision analysis for offshore wind energy potential in Egypt. Renew. Energy 118, 278–289.
Mukut, A.M.I., Islam, M.Q., Alam, M.M., 2008. Analysis of wind characteristics in coastal areas of Bangladesh. J. Mech. Eng. 39, 45–49.
Oh, K.-Y., Kim, J.-Y., Lee, J.-K., Ryu, M.-S., Lee, J.-S., 2012. An assessment of wind energy potential at the demonstration offshore wind farm in Korea. Energy Energy Exergy Model. Adv. Energy Syst. 46, 555–563.
de Oliveira, M.M.F., Ebecken, N.F.F., de Oliveira, J.L.F., Gilleland, E., 2011. Generalized extreme wind speed distributions in South America over the Atlantic Ocean region. Theor. Appl. Climatol. 104, 377–385.
Pagnini, L.C., Burlando, M., Repetto, M.P., 2015. Experimental power curve of small-size wind turbines in turbulent urban environment. Appl. Energy 154, 112–121.
Peng, W., Huang, X., Fan, Y., Zhang, J., Ren, X., 2017. Numerical analysis and performance optimization of a submerged wave energy converting device based on the floating breakwater. J. Renew. Sustain. Energy 9, 044503.
Pérez, I.A., García, M.A., Sánchez, M.L., de Torre, B., 2004. Analysis of height variations of sodar-derived wind speeds in Northern Spain. J. Wind Eng. Ind. Aerodyn. 92, 875–894.
Perrin, O., Rootzén, H., Taesler, R., 2006. A discussion of statistical methods used to estimate extreme wind speeds. Theor. Appl. Climatol. 85, 203–215.
Qiu, Y., Anadon, L.D., 2012. The price of wind power in China during its expansion: Technology adoption, learning-by-doing, economies of scale, and manufacturing localization. Energy Econ. 34, 772–785.
Rodrigues, S., Chen, X., Morgado-Dias, F., 2017. Economic analysis of photovoltaic systems for the residential market under China's new regulation. Energy Policy 101, 467–472.
Saeidi, D., Sedaghat, A., Alamdari, P., Alemrajabi, A.A., 2013. Aerodynamic design and economical evaluation of site specific small vertical axis wind turbines. Appl. Energy 101, 765–775.
Shu, Z.R., Li, Q.S., Chan, P.W., 2015a. Statistical analysis of wind characteristics and wind energy potential in Hong Kong. Energy Convers. Manag. 101, 644–657.
Shu, Z.R., Li, Q.S., Chan, P.W., 2015b. Investigation of offshore wind energy potential in Hong Kong based on Weibull distribution function. Appl. Energy 156, 362–373.
Shu, Z.R., Li, Q.S., He, Y.C., Chan, P.W., 2016. Observations of offshore wind characteristics by Doppler-LiDAR for wind energy applications. Appl. Energy 169, 150–163.
Song, L., Chen, W., Wang, B., Zhi, S., Liu, A., 2016. Characteristics of wind profiles in the landfalling typhoon boundary layer. J. Wind Eng. Ind. Aerodyn. 149, 77–88.
Stewart, J.Q., Whiteman, C.D., Steenburgh, W.J., Bian, X., 2002. A climatological study of thermally driven wind systems of the U.S. Intermountain West. Bull. Am. Meteorol. Soc. 83, 699–708.
Ti, Z., Wei, K., Li, Y., Xu, B., 2020. Effect of wave spectral variability on stochastic response of a long-span bridge subjected to random waves during Tropical cyclones. J. Bridge Eng. 25, 04019131.
Ti, Z., Zhang, M., Li, Y., Wei, K., 2019. Numerical study on the stochastic response of a long-span sea-crossing bridge subjected to extreme nonlinear wave loads. Eng. Struct. 196, 109287.
Tieleman, H.W., 2008. Strong wind observations in the atmospheric surface layer. J. Wind Eng. Ind. Aerodyn. 96, 41–77.
Tu, Q., Betz, R., Mo, J., Fan, Y., Liu, Y., 2019. Achieving grid parity of wind power in China – present levelized cost of electricity and future evolution. Appl. Energy 250, 1053–1064.
Wulfmeyer, V., Janjić, T., 2005. Twenty-four-hour observations of the marine boundary layer using shipborne NOAA high-resolution Doppler lidar. J. Appl. Meteorol. 44, 1723–1744.
Xia, J., Hong, T., Shen, Q., Feng, W., Yang, L., Im, P., Lu, A., Bhandari, M., 2014. Comparison of building energy use data between the United States and China. Energy Build. 78, 165–175.
Xing, Y., Ree, R.H., 2017. Uplift-driven diversification in the Hengduan Mountains, a temperate biodiversity hotspot. Proc. Natl. Acad. Sci. 114, E3444–E3451.
Zhang, J., Wei, K., Qin, S., 2019a. An efficient numerical model for hydrodynamic added mass of immersed column with arbitrary cross - section. Ocean Eng. 187, 106192.
Zhang, M., Yu, J., Zhang, J., Wu, L., Li, Y., 2019b. Study on the wind-field characteristics over a bridge site due to the shielding effects of mountains in a deep gorge via numerical simulation. Adv. Struct. Eng. 22, 3055–3065.
Zhang, J., Zhang, M., Li, Y., Fang, C., 2020. Comparison of wind characteristics at different heights of deep-cut canyon based on field measurement. Adv. Struct. Eng. 23, 219–233.